

Local electrical potential detection of DNA by nanowire–nanopore sensors

Ping Xie¹, Qihua Xiong^{2,3}, Ying Fang⁴, Quan Qing¹ and Charles M. Lieber^{1,5*}

Nanopores could potentially be used to perform single-molecule DNA sequencing at low cost and with high throughput^{1–4}. Although single base resolution and differentiation have been demonstrated with nanopores using ionic current measurements^{5–7}, direct sequencing has not been achieved because of the difficulties in recording very small (\sim pA) ionic currents at a bandwidth consistent with fast translocation speeds^{1–3}. Here, we show that solid-state nanopores can be combined with silicon nanowire field-effect transistors to create sensors in which detection is localized and self-aligned at the nanopore. Well-defined field-effect transistor signals associated with DNA translocation are recorded when an ionic strength gradient is imposed across the nanopores. Measurements and modelling show that field-effect transistor signals are generated by highly localized changes in the electrical potential during DNA translocation, and that nanowire–nanopore sensors could enable large-scale integration with a high intrinsic bandwidth.

Most current nanopore technology is based on detecting a modulation in the ionic current due to the partial blockade of a nanopore during DNA translocation^{1–4}. Significant progress has been made towards direct DNA sequencing during translocation through protein nanopore engineering^{5,6} and novel membrane materials^{7–9}, although some challenges remain^{1,3}. For example, the DNA translocation speed, $\sim 1 \mu\text{s base}^{-1}$, is faster than the bandwidth electronics available to amplify the small ionic current, and it is difficult to record ionic current from individual nanopores in a highly parallel multiplexed format. To overcome these issues, methods have been developed to better control the translocation^{4,10–13}, thus enabling potential reductions in translocation speed that could facilitate ionic current detection. Simultaneously, new detection designs have been proposed that could allow the recording of larger and local signals from sensors integrated with the nanopore^{1–3}. These integrated sensors include devices based on the measurement of capacitive coupling¹⁴ and tunnelling currents^{15–17}, although none has yet improved upon traditional ionic current detection in experiments. Field-effect transistors (FETs), including nanowire and carbon-nanotube FETs, have demonstrated high intrinsic speeds^{18,19} and high sensitivities as chemical and biological sensors^{20–22}, and thus might also function as integrated detectors for nanopores. However, the lack of a clear mechanism for FET-based detection of DNA during nanopore translocation (where the relatively high solution ionic strength is expected to screen the detection of molecular charge previously used in sensing experiments^{20,21}) has left these detectors largely unexplored.

We investigated the possibility of integrating a FET with a nanopore using synthesized silicon nanowires as the nanoscale FETs^{20–22}.

The integrated nanowire–nanopore FET sensor comprises a short-channel silicon nanowire FET on a silicon nitride (SiN_x) membrane-based chip, with the nanopore extending through both the nanowire edge and the SiN_x membrane support (Fig. 1a, Supplementary Fig. S1). The fabrication of nanowire–nanopore FET sensors involves several key steps (Supplementary Methods). First, p-type silicon nanowires FETs were fabricated on SiN_x membranes with nickel-metal source–drain contacts with a typical spacing of 1–2 μm . To minimize signal attenuation due to FET-channel series resistance, the active length of the silicon nanowire was further reduced to less than 200 nm by solid-state diffusion to form metallic nickel silicide (NiSi) contacts¹⁹ (Fig. 1b, inset). Next, a focused electron beam (via transmission electron microscopy, TEM) was used to form a nanopore²³ through the edge of the silicon nanowire and the underlying membrane (Fig. 1b).

The sensitivity of nanowire–nanopore FET sensors fabricated in this way was characterized by scanning gate microscopy (SGM) (Supplementary Methods). A SGM map of the conductance change versus biased tip position for a silicon nanowire FET device after nanopore formation (Fig. 1c) shows a pronounced peak of conductance change localized around the nanopore position and no response from the NiSi region of the nanowire device. The sensitivity (conductance change/tip voltage) along the nanowire (Fig. 1d, red line) exhibits a maximum of 18 nS V^{-1} , which is sharply localized and aligned with the nanopore position at approximately the midpoint along the length of the semiconductor channel. We note that the sensitivity of this device before nanopore formation is relatively constant ($5\text{--}8 \text{ nS V}^{-1}$; Fig. 1d, black line) along the entire active silicon channel. The larger than twofold sensitivity enhancement can be explained qualitatively by the increase in channel resistance of the nanopore portion of the silicon nanowire FET where silicon is removed. Although additional work will be needed to quantify the factors contributing to this observed enhancement, the localized sensitivity makes the nanowire–nanopore FET attractive for monitoring translocation events through the nanopore.

Single-channel DNA translocation measurements were carried out with two polydimethylsiloxane (PDMS) solution chambers as *trans* and *cis* reservoirs above and below the SiN_x membrane, respectively. Both chambers were filled with 1 M KCl buffer, as typically used in nanopore experiments^{24,25}. Following injection of 6 nM, $\sim 2.6 \text{ kbps}$ linear double-stranded DNA (dsDNA) (pUC19; Supplementary Methods) into the *cis* chamber, we observed translocation events in the ionic current channel when the transmembrane voltage reached $\sim 0.6 \text{ V}$ (Fig. 2a, top panel). Simultaneous recording of the nanowire FET conductance (Fig. 2a, lower panel) showed no noticeable translocation signals and only small and slow conductance baseline shifts. However, if the *trans*

¹Department of Chemistry and Chemical Biology, Harvard University, Cambridge, Massachusetts 02138, USA, ²Division of Physics and Applied Physics, School of Physical and Mathematical Sciences, Nanyang Technological University, Singapore 637371, Singapore, ³Division of Microelectronics, School of Electrical and Electronic Engineering, Nanyang Technological University, Singapore 619798, Singapore, ⁴National Center for Nanoscience and Technology, China, Beijing 100910, PR China, ⁵School of Engineering and Applied Sciences, Harvard University, Cambridge, Massachusetts 02138, USA. *e-mail: cml@cmliris.harvard.edu

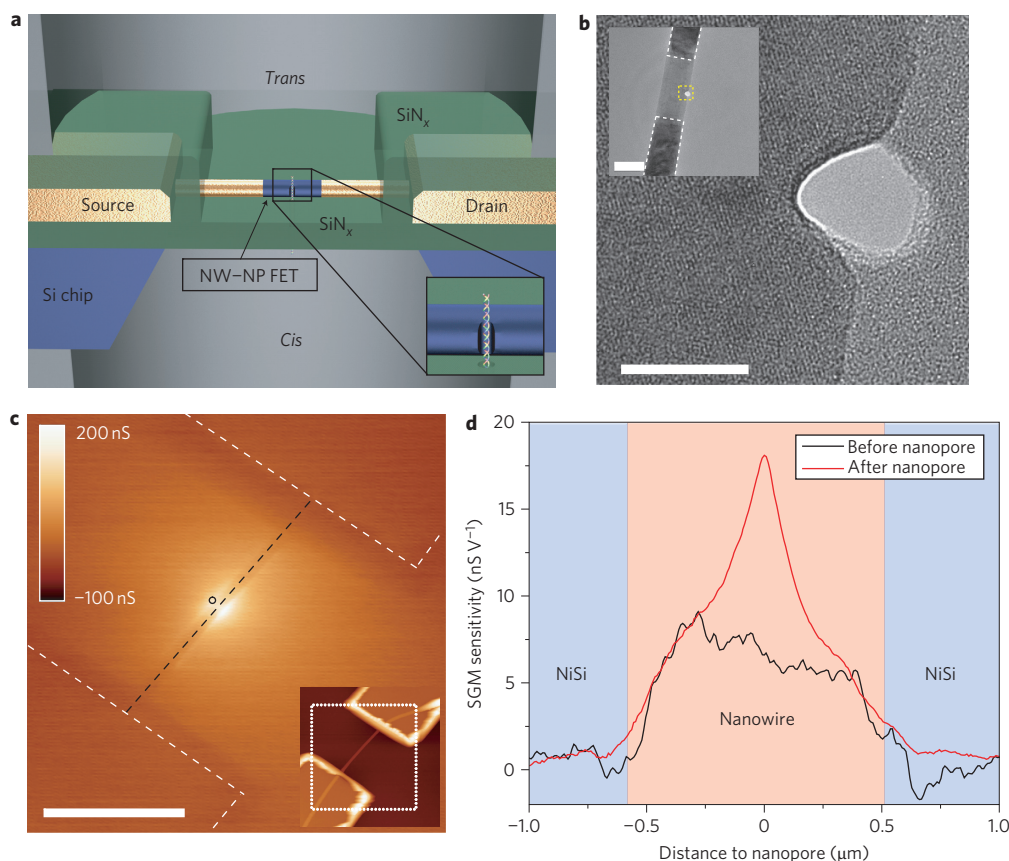


Figure 1 | Nanowire-nanopore transistor. **a**, Schematic of the nanowire-nanopore measurement set-up. Inset: zoom-in view around the nanopore. NW-NP, nanowire-nanopore. **b**, High-resolution TEM image of a silicon nanowire with the nanopore off-axis at the nanowire edge. Scale bar, 10 nm. Inset: larger-scale TEM image of a nanowire-nanopore FET device showing the central silicon nanowire connected to darker NiSi contacts, which are indicated by the white dashed line. The region where the high-resolution TEM image was recorded is indicated by the yellow dashed square. Scale bar (inset), 50 nm. **c**, SGM image of a silicon nanowire-nanopore device recorded with the tip voltage at -10 V. Scale bar, $1\ \mu\text{m}$. Nanopore position is indicated by the black circle. Nickel contacts are indicated by white dashed lines and the nanowire between the two contacts is indicated by the black dashed line. Inset: AFM topographic image of the device, with the SGM image area indicated by the white square. Colour scale (-100 to 200 nS) corresponds to the conductance change. **d**, Scanning gate sensitivity profile of the same device before and after nanopore formation, with the profile taken along the black dashed line in **c**, and averaged over an ~ 100 nm width perpendicular to the dashed line.

(nanowire-nanopore FET side) and *cis* (back side) chambers are filled with solutions of different ionic strength (for example, 10 mM in the *trans* chamber and 1 M in *cis* chamber), clear FET conductance signals with perfect time correlation to ionic current events can be observed (Fig. 2b) for a voltage of ~ 2 V. Qualitatively, a larger voltage is expected given the lower solution resistance and therefore lower electric field on the *cis* side, which determines DNA entry into the nanopore³. With a further increase in the voltage to 2.4 V (Fig. 2c), the duration of translocation events in both ionic current and FET channels decreased, while the frequency increased. These changes in duration and frequency are consistent with the previous results reported for ionic current events recorded in other nanopore experiments^{10,24}. Importantly, the change in the FET signal during translocation—a decrease in conductance—is opposite to that expected for charge-based sensing of the DNA with a p-type semiconductor²⁰, therefore implying a new detection mechanism.

The amplitude of the nanowire-nanopore FET signal in a non-balanced buffer salt concentration can be compared to the ionic current signal by converting the FET conductance to a current. This conversion shows that the FET current change is ~ 30 nA compared with the ~ 3 nA ionic current changes during DNA translocation. Although the noise in this nanowire-nanopore FET (Fig. 2) is relatively high, other nanowire-nanopore

FETs (Fig. 4b) and other silicon nanowire FET sensors^{26,27} demonstrate that much lower noise (and correspondingly higher signal-to-noise ratio) can be achieved in general for nanowire-nanopore FETs. In addition, the relatively large (30 nA) translocation signal from the FET suggests the potential for higher-bandwidth recording than with smaller ionic-current detection schemes.

To understand the nanowire-nanopore detection mechanism we first consider basic experimental facts. First, and as discussed above, it is possible to exclude direct charge sensing by the nanowire-nanopore FET^{20,21}, because the negative charge on the DNA backbone should produce an increase in conductance for the p-type device during translocation instead of the observed decrease. Second, the importance of the differential buffer salt concentration suggests that solution resistance plays an important role in the signal generation. Specifically, under balanced buffer conditions (1 M/1 M), the nanopore dominates the solution resistance and the voltage drops primarily across the nanopore. The potential around the nanowire-nanopore sensor is very close to ground, regardless of the change in solution resistance during DNA translocation. However, when the buffer concentration in the *trans* chamber containing the nanowire-nanopore sensor is lower than that of the *cis* chamber, the nanopore and *trans* chamber solution resistances are

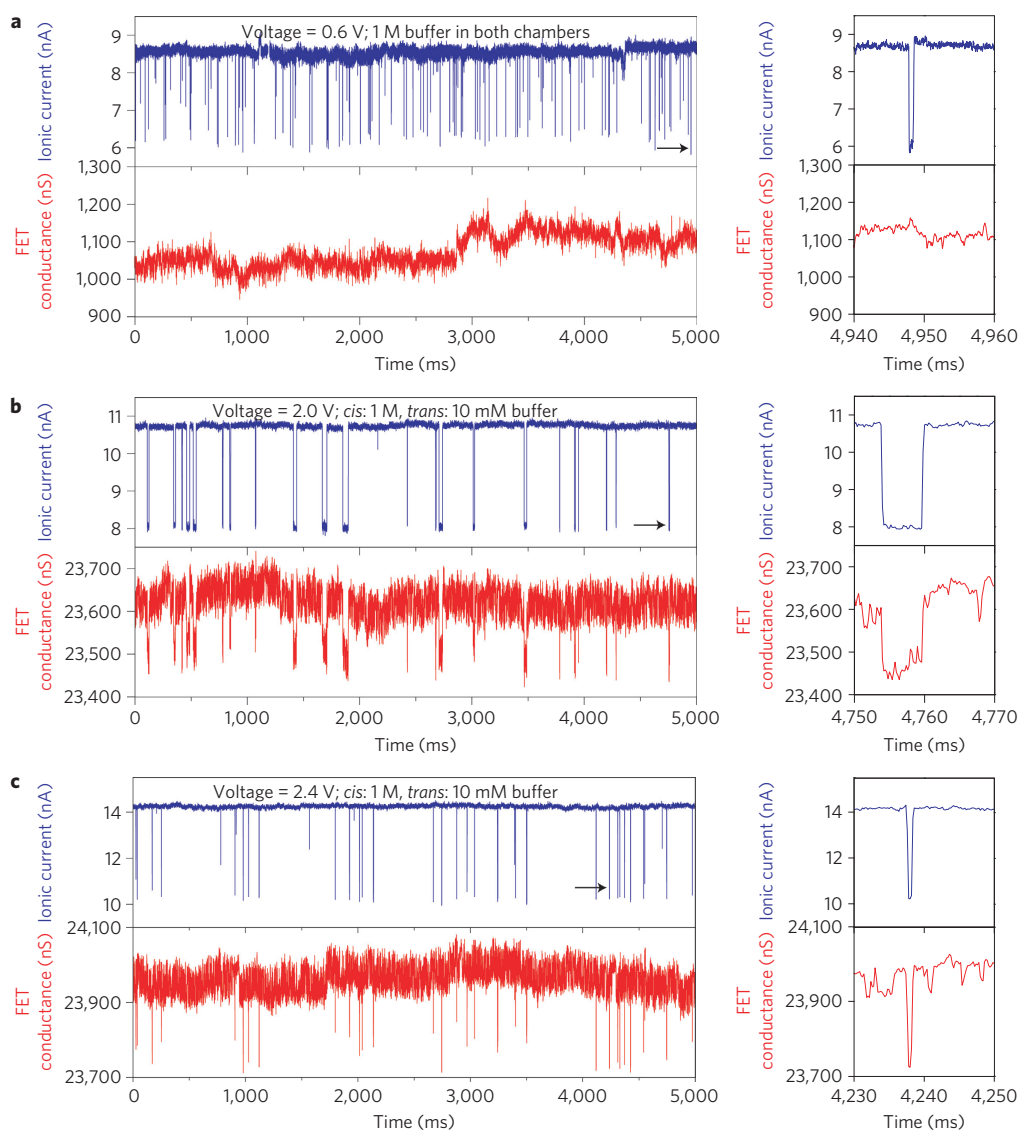


Figure 2 | Single-channel nanowire-nanopore FET detection of DNA translocation. **a–c**, Left panels: simultaneously recorded ionic current and FET conductance signals with both chambers filled with 1 M KCl buffer, voltage 0.6 V and 6 nM pUC 19 dsDNA in the *cis* chamber (**a**); simultaneously recorded ionic current and FET conductance signals at 2 V voltage (**b**); simultaneously recorded ionic current and FET conductance signals at 2.4 V voltage (**c**). Measurements in **b** and **c** were carried out with a *trans* chamber KCl buffer concentration of 10 mM, *cis* chamber KCl buffer concentration of 1 M, and 1.4 nM pUC19 DNA. Right panels: zoom-in views of single ionic current and FET conductance events at the time indicated by black arrows in the ionic current traces of the corresponding left panels.

comparable and the resistance of the *cis* chamber will be negligible. Hence, changes in the solution resistance of the nanopore and *trans* chamber during DNA translocation can result in a change in the potential around the nanowire–nanopore sensor, which is then detected.

To understand quantitatively this proposed and unexpected detection mechanism for the nanowire–nanopore FET, we modelled the buffer concentration, electric potential and electric field distributions inside the solution of the nanopore and solution chamber system (Fig. 3a). The equivalent circuit (Fig. 3b) separates the total solution resistance into nanopore resistance (R_{pore}), and *cis* and *trans* chamber access resistances (R_{trans} and R_{cis} respectively). The nanowire–nanopore FET sensor is simplified as a point-like potential detector at the nanopore opening on the *trans* side. Translocation of DNA molecules through the nanopore will partially block the nanopore, thus leading to a transient change in nanopore resistance and both chamber access resistances. Detailed calculations (Supplementary Methods, Fig. S2) provide the solution

electrical potential change around the *trans* chamber nanopore opening (potential change signal) during DNA translocation as

$$\delta V \approx \frac{2VA(4l + d)(C_{\text{cis}}/C_{\text{trans}} - 1)}{\pi \ln(C_{\text{cis}}/C_{\text{trans}})(2l + d)(d^2(C_{\text{cis}}/C_{\text{trans}} - 1) + 4(2l + d)r)} \quad (1)$$

Here V , A , l , d , C_{cis} , C_{trans} and r are the voltage, cross-sectional area of the DNA, membrane thickness, nanopore diameter, *cis* and *trans* chamber buffer salt concentrations and distance to the nanopore opening, respectively.

To further analyse the potential change signal, we first plot the signal at the nanopore opening as a function of nanopore diameter and *cis*/*trans* chamber buffer concentration ratio (Fig. 3c). The potential change is predicted to increase with decreasing nanopore diameter, and can reach more than 10% of the applied voltage when the nanopore diameter is ~ 2 nm. The maximal potential change

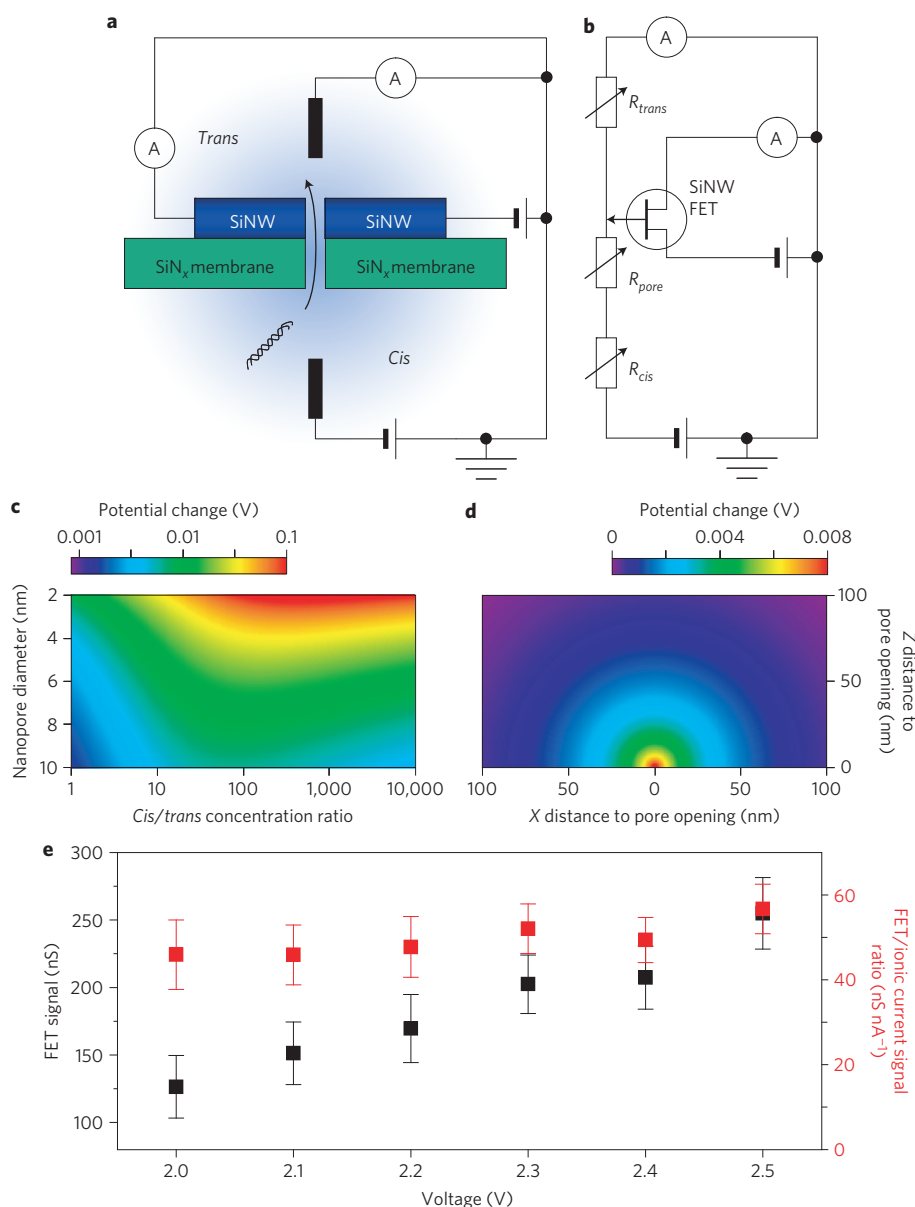


Figure 3 | Nanowire-nanopore sensing mechanism. **a**, Schematic of the sensing circuit. **b**, Equivalent circuit diagram for **a**. SiNW, silicon nanowire. **c**, Calculated potential change at the nanopore opening in the *trans* chamber (using Supplementary equation (9)), due to translocation of one dsDNA molecule at a voltage of 1 V as a function of nanopore diameter and *cis/trans* chamber buffer concentration ratio. **d**, Calculated potential change distribution in the *trans* chamber for a 10-nm-diameter nanopore at 1 V voltage (equation (1)). **e**, Experimental values of the FET signal (black data points) and FET signal/ionic current signal ratio (red data points) under different voltages.

signal for a given diameter nanopore is also predicted to occur at intermediate buffer concentration ratios. Specifically, for the nanopore geometry used in our experiments (diameter, 7–10 nm; membrane thickness, 50 nm), the potential change signal can be larger than 1% of the voltage at the optimal buffer concentration ratio (~100:1). We have tested the consistency of the model predictions with our experiments. Specifically, conversion of the FET conductance signal into potential change using the measured solution-gated transconductance²⁷ yields a potential change of 25 mV (Fig. 2c), which agrees with our model calculations (31–16 mV, with a 7–10-nm-diameter nanopore, and all other conditions the same as in the experiment).

In addition, the predicted distribution of the potential change in the *trans* chamber at this optimal condition (Fig. 3d) shows a highly localized signal within several tens of nanometres of the nanopore, suggesting the possibility of high-density integration of

nanowire-nanopore sensors without crosstalk. Moreover, analysis of the voltage drops across the nanopore and both chambers allows their solution resistances to be compared. To do so, we plotted the potential distribution in both chambers at the optimal buffer concentration ratio (Supplementary Fig. S3), and found that the access resistance of the *trans* chamber and the resistance of the nanopore are indeed within the same order of magnitude, whereas the access resistance of the *cis* chamber is negligible. From the signal distribution, we can also roughly estimate the intrinsic bandwidth of the potential change signal (Supplementary Methods, Fig. S4). A simple RC model suggests a potential signal bandwidth of ~1 GHz under our experimental conditions. Finally, the different voltages required to initiate translocation at 1:1 and 100:1 buffer concentration ratios (Fig. 2) can be explained quantitatively by our model: the onset of translocation is determined by the electric field at the nanopore opening in the *cis* chamber, which

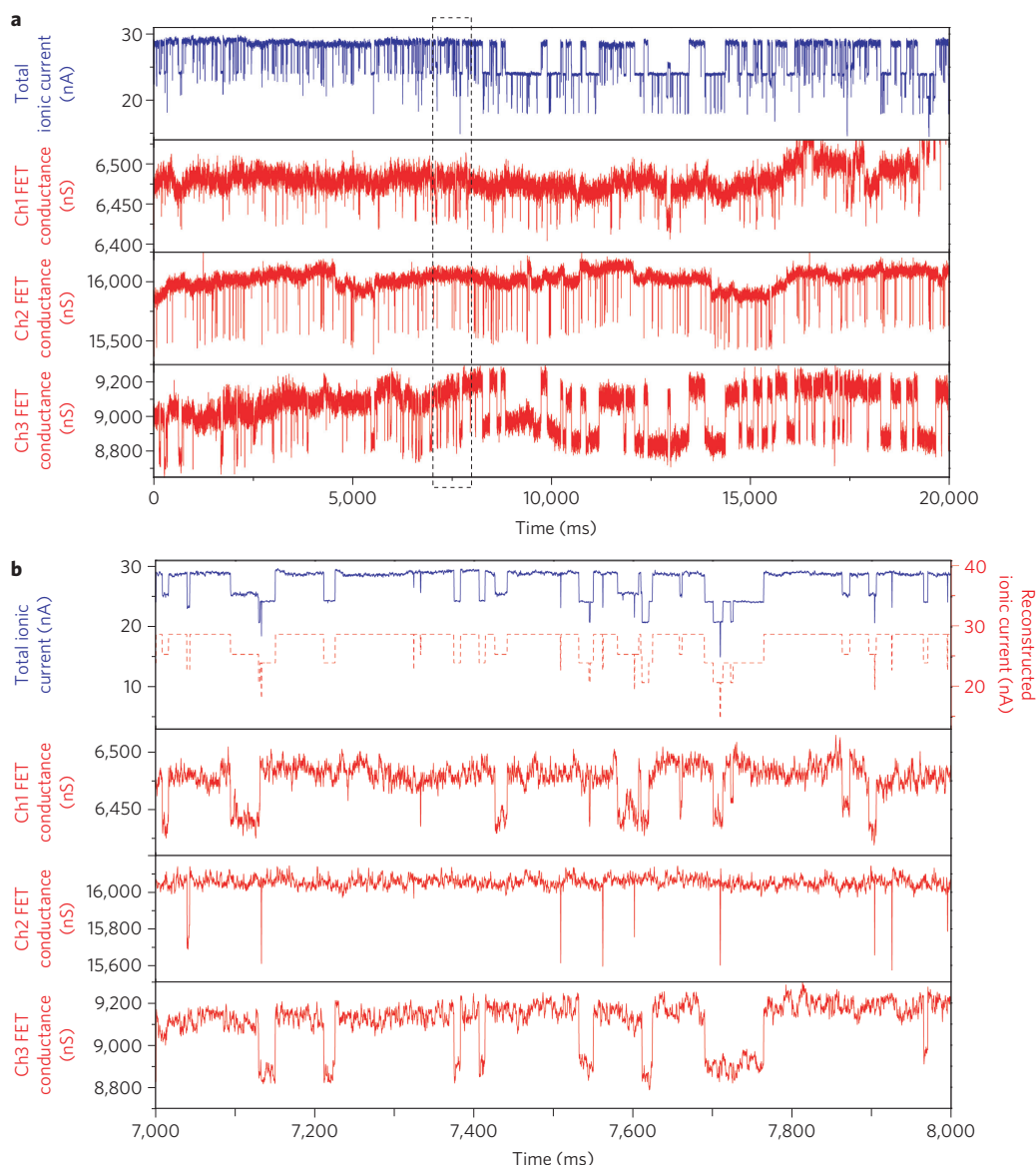


Figure 4 | Multi-channel recording of DNA translocation with three nanowire-nanopore FET sensors. All measurements are made with 1 M KCl buffer in the *cis* chamber and 10 mM KCl buffer in the *trans* chamber, a voltage of 3 V, and 1.4 nM pUC19 DNA. **a**, Simultaneous recording of the total ionic current and three nanowire-nanopore FET conductance channels (Ch1–Ch3). **b**, Higher-resolution view of the multiplexed recording from the dashed rectangular area in **a**. The dashed red trace in the upper panel corresponds to the reconstructed ionic current trace (offset 10 nA for clarity) calculated from the three FET traces.

pulls the negatively charged DNA into the nanopore. We plotted the electric potential and field distribution inside the nanopore for both 1:1 and 100:1 buffer concentration ratios (Supplementary Fig. S5). For the 1:1 case, the field ($\sim 1.8 \times 10^7 \text{ V m}^{-1}$) is uniformly distributed within the nanopore, but for the 100:1 case, the field ($\sim 0.45 \times 10^7 \text{ V m}^{-1}$) is smaller on the *cis* side because of the lower resistance (owing to higher buffer concentration) there. To produce the same electric field, the voltage applied for the 100:1 case should be approximately four times higher than the voltage for the 1:1 case, which is quantitatively consistent with the observed onset of translocation events at $\sim 2 \text{ V}$ and $0.5\text{--}0.6 \text{ V}$, respectively (Fig. 2).

A crucial difference between our FET-based local potential sensing and other proposed DNA direct sensing mechanisms^{8–17} is the dependence of the FET signal on the ionic current signal and the voltage. For DNA sensing mechanisms that rely on the direct interaction between DNA and the sensor through electrical coupling⁸ or quantum-mechanical tunnelling^{15,16}, the signal is typically not related directly to the ionic current or voltage and

should not change significantly when the voltage changes. For the local potential sensing mechanism, however, the sensor signal is predicted to be proportional to the voltage and can be regarded as the linear amplification of the ionic current signal. Hence, the ratio between the FET signal and the ionic current signal should be constant for a given nanopore geometry and buffer concentration (Supplementary Methods). This unique feature was experimentally tested by plotting the FET signal amplitude (Fig. 3e, black) and FET/ionic current signal ratio (Fig. 3e, red) at different voltage values. Notably, the data show that the FET signal amplitude increases, but the signal ratio is approximately constant with increasing voltage, and thus provides strong support for sensing by a local potential mechanism.

We have also carried out several additional experiments to test the validity of our new model. First, DNA translocation experiments were carried out at different buffer salt concentrations in the *cis/trans* chambers (Supplementary Methods, Figs S6,S7). Measurements made at 3.3 M/33 mM (which equates to the same

100:1 ratio as for the results presented in Fig. 4 for 1 M/10 mM) show that the signal amplitude is approximately constant when the buffer concentration changes proportionally in both chambers, in agreement with the model predictions and in contrast to the conventional charge-based FET sensing mechanism. Furthermore, when the *cis/trans* concentration ratio is reduced to 10:1, the recorded translocation signal (Supplementary Fig. S7) is reduced as predicted by the model in Fig. 3c. Finally, translocation experiments carried using the formally neutral polymer polyethylene glycol (Supplementary Methods, Fig. S8) show correlated ionic current and FET conductance signals similar to but smaller in amplitude than recorded for DNA translocation. The smaller FET signal is consistent with expectations for our model (given the smaller ionic current signal change) and, more importantly, the fact that we observe the same signal polarity in the FET channel is inconsistent with a charge-based FET sensing mechanism but in complete agreement with our potential sensing mechanism.

A key advantage of the nanowire–nanopore FET sensor is the potential for integration and multiplexing within a single analysis chamber without complex microfluidic systems²⁸. Notably, simultaneous recording from three nanowire–nanopore devices (Fig. 4a) demonstrates that continuous translocation events are observed in all three FET channels as well as for the total ionic current channel. Closer examination of the three FET and total ionic current signals (Fig. 4b) shows clearly that the three FET channels operate independently, and every falling or rising edge apparent in the total ionic current channel can be uniquely correlated to a corresponding edge in one of the three FET channels. Significantly, the total ionic current signal reconstructed from the data for the three FET channels (dashed-red trace, top panel, Fig. 4b) exhibits nearly perfect agreement with the measured total ionic current (Supplementary Methods). In addition, a histogram of channel-specific ionic currents (Supplementary Methods, Fig. S9) demonstrates that the ionic current signal amplitudes in different channels are also independent. As previous studies have shown that it is possible to fabricate large numbers of nanowire–FET devices²⁹ with reproducible properties, and the local potential signal decay length is as short as tens of nanometres, we expect that it will also be possible to multiplex the nanowire–nanopore FETs in much higher numbers and densities.

Direct sequencing of long single-stranded DNA molecules using FET-based nanopore sensors and the new potential change detection mechanism will require optimization of the signal-to-noise ratio associated with individual bases as well as improvement in signal spatial resolution. Recognizing that direct base differentiation by FET potential measurement is coupled to variations in the ionic current suggests that concepts proposed and demonstrated for base-resolved ionic current measurements^{5–7} could be successfully combined with our work. For example, it should be possible to extend our nanowire–nanopore FET to atomically thin graphene membranes^{7–9} so as to achieve single base spatial resolution, although the graphene nanopore would require precise structure engineering to enable differentiation of the distinct bases. Alternatively, coupling an engineered protein nanopore to the nanowire–nanopore FET could provide both the spatial and base resolution necessary for direct sequencing due to the localized change of the potential at the nanopore opening (Fig. 3d). Our nanowire–nanopore FET sensor results and modelling strongly motivate such effort, given the advantages over direct ionic current and other sensor-based detection schemes, including larger measurement signals, high signal bandwidth with attractive nanopore-size scaling, and straightforward integration and multiplexing. We believe that this work provides a strong starting point for a new class of nanopore sequencing devices with the capability for fast direct sequencing and large-scale integration.

Methods

The silicon nanowires were synthesized by chemical vapour deposition (CVD) methods as described previously³⁰. Electron-beam lithography (EBL) and solid-state diffusion of the nickel contact were used to fabricate short-channel devices on commercially available SiN_x TEM membrane grid chips. A SiN_x conformal thin film deposited by plasma-enhanced CVD was used to passivate all metal electrodes before final lift-off. Nanopores were drilled by focusing the 200 keV electron beam in a JEOL 2010F field-emission TEM. The nanowire–nanopore FET sensor chip was glued onto a home-made PCB chip carrier and electrically connected to the chip carrier by wire bonding. The chip carrier was sandwiched between mechanically clamped-on PDMS chambers with a tight seal, which were filled with sterilized and filtered buffer solutions. DNA translocation measurements were made using linearized pUC19. FET and ionic current signals were amplified and digitized using standard electronics with the sensor set-up mounted in a Faraday box.

See supplementary information for full methods and any associated references.

Received 16 September 2011; accepted 7 November 2011;
published online 11 December 2011

References

- Branton, D. *et al.* The potential and challenges of nanopore sequencing. *Nature Biotechnol.* **26**, 1146–1153 (2008).
- Venkatesan, B. M. & Bashir R. Nanopore sensors for nucleic acid analysis. *Nature Nanotech.* **6**, 615–624 (2011).
- Zwolak, M. & Ventra, M. D. Colloquium: physical approaches to DNA sequencing and detection. *Rev. Mod. Phys.* **80**, 141–163 (2008).
- Dekker, C. Solid-state nanopores. *Nature Nanotech.* **2**, 209–215 (2007).
- Clarke, J. *et al.* Continuous base identification for single-molecule nanopore DNA sequencing. *Nature Nanotech.* **4**, 265–270 (2009).
- Derrington, I. M. *et al.* Nanopore DNA sequencing with MspA. *Proc. Natl Acad. Sci. USA* **107**, 16060–16065 (2010).
- Garaj, S. *et al.* Graphene as a subnanometre trans-electrode membrane. *Nature* **467**, 190–193 (2010).
- Merchant, C. A. *et al.* DNA translocation through graphene nanopores. *Nano Lett.* **10**, 2915–2921 (2010).
- Schneider, G. F. *et al.* DNA translocation through graphene nanopores. *Nano Lett.* **10**, 3163–3167 (2010).
- Fologea, D., Uplinger, J., Thomas, B., McNabb, D. S. & Li, J. Slowing DNA translocation in a solid-state nanopore. *Nano Lett.* **5**, 1734–1737 (2005).
- Peng, H. & Ling X. S. Reverse DNA translocation through a solid-state nanopore by magnetic tweezers. *Nanotechnology* **20**, 185101 (2009).
- Olasagasti, F. *et al.* Replication of individual DNA molecules under electronic control using a protein nanopore. *Nature Nanotech.* **5**, 798–806 (2010).
- Luan, B. *et al.* Base-by-base ratcheting of single stranded DNA through a solid-state nanopore. *Phys. Rev. Lett.* **104**, 238103 (2010).
- Gracheva, M. E. *et al.* Simulation of the electric response of DNA translocation through a semiconductor nanopore-capacitor. *Nanotechnology* **17**, 622–633 (2006).
- King, G. M. & Golovchenko, J. A. Probing nanotube–nanopore interactions. *Phys. Rev. Lett.* **95**, 216103 (2005).
- Lagerqvist, J., Zwolak, M. & Ventra, M. D. Fast DNA sequencing via transverse electronic transport. *Nano Lett.* **6**, 779–782 (2006).
- Ivanov, A. P. *et al.* DNA tunnelling detector embedded in a nanopore. *Nano Lett.* **11**, 279–285 (2011).
- Chaste, J. *et al.* Single carbon nanotube transistor at GHz frequency. *Nano Lett.* **8**, 525–528 (2008).
- Hu, Y., Xiang, J., Liang, G., Yan, H. & Lieber, C. M. Sub-100 nanometer channel length Ge/Si nanowire transistors with potential for 2 THz switching speed. *Nano Lett.* **8**, 925–930 (2008).
- Cui, Y., Wei, Q., Park, H. & Lieber, C. M. Nanowire nanosensors for highly sensitive and selective detection of biological and chemical species. *Science* **293**, 1289–1292 (2001).
- Patolsky, F. *et al.* Electrical detection of single viruses. *Proc. Natl Acad. Sci. USA* **101**, 14017–14022 (2004).
- Patolsky, F. *et al.* Detection, stimulation, and inhibition of neuronal signals with high-density nanowire transistor arrays. *Science* **313**, 1100–1104 (2006).
- Kim, M. J., Wanunu, M., Bell, D. C. & Meller, A. Rapid fabrication of uniformly sized nanopores and nanopore arrays for parallel DNA analysis. *Adv. Mater.* **18**, 3149–3153 (2006).
- Kasianowicz, J. J., Brandin, E., Branton, D. & Deamer, D. W. Characterization of individual polynucleotide molecules using a membrane channel. *Proc. Natl Acad. Sci. USA* **93**, 13770–13773 (1996).
- Li, J. *et al.* Ion-beam sculpting at nanometre length scales. *Nature* **412**, 166–169 (2001).
- Cohen-Karni, T., Timko, B. P., Weiss, L. E. & Lieber, C. M. Flexible electrical recording from cells using nanowire transistor arrays. *Proc. Natl Acad. Sci. USA* **106**, 7309–7313 (2009).
- Tian, B. *et al.* Three-dimensional, flexible nanoscale field-effect transistors as localised bioprobes. *Science* **329**, 831–834 (2010).

28. Osaki, T., Suzuki H., Le Pioutle, B. & Takeuchi, S. Multichannel simultaneous measurements of single-molecule translocation in α -hemolysin nanopore array. *Anal. Chem.* **81**, 9866–9870 (2009).
29. Yan, H. *et al.* Programmable nanowire circuits for nanoprocessors. *Nature* **470**, 240–244 (2011).
30. Cui, Y., Zhong, Z., Wang D., Wang, W. & Lieber, C. M. High performance silicon nanowire field effect transistors. *Nano Lett.* **3**, 149–152 (2003).

Acknowledgements

The authors thank A. Meller, M. Wanunu, D. Casanova, J. Huang, J. Cahoon and T.J. Kempa for helpful discussions. C.M.L. acknowledges support of this work from a NIH Director's Pioneer Award (5DP1OD003900).

Author contributions

P.X., Q.X., Y.F. and C.M.L. designed the experiments. P.X., Q.X. and Y.F. performed the experiments. P.X. performed the modelling and calculation. P.X. and Q.Q. wrote the program for data processing. P.X., Q.X., Y.F., Q.Q. and C.M.L. analysed the data and wrote the manuscript.

Additional information

The authors declare no competing financial interests. Supplementary information accompanies this paper at www.nature.com/naturenanotechnology. Reprints and permission information is available online at <http://www.nature.com/reprints>. Correspondence and requests for materials should be addressed to C.M.L.